Bioorganic Chemistry 150 (2024) 107595

Contents lists available at ScienceDirect

Bioorganic Chemistry

journal homepage: www.elsevier.com/locate/bioorg

RNase H-sensitive multifunctional ASO-based constructs as promising tools for the treatment of multifactorial complex pathologies

Aida Mata-Ventosa [a,b,c,1], Ariadna Vila-Planas [d,1], Aina Solsona-Pujol [d,e,f], Jordi de la Dueña [d], Maria Torrents [d], Eduardo Izquierdo-García [d], Marçal Pastor-Anglada [a,b,c], Sandra Pérez-Torras [a,b,c,*], Montserrat Terrazas [d,*]

[a] Molecular Pharmacology and Experimental Therapeutics, Department of Biochemistry and Molecular Biomedicine, Institute of Biomedicine, University of Barcelona (IBUB), Barcelona, Spain
[b] Centro de Investigación Biomédica en Red de Enfermedades Hepáticas y Digestivas (CIBER EHD), Instituto de Salud Carlos III, Madrid, Spain
[c] Institut de Recerca Sant Joan de Déu (IR SJD-CERCA), Esplugues de Llobregat, Barcelona, Spain
[d] Department of Inorganic and Organic Chemistry, Organic Chemistry Section, Institute of Biomedicine, University of Barcelona (IBUB), Barcelona, Spain
[e] BioFrontiers Institute, University of Colorado, Boulder, CO, United States
[f] Department of Chemical and Biological Engineering, University of Colorado, Boulder, CO, United States

ARTICLE INFO

Keywords:
3ASO multitargeting tool
Antisense oligonucleotides
Stimuli-responsive
RNase H
Complex pathologies
Cancer

ABSTRACT

Combined therapies play a key role in the fight against complex pathologies, such as cancer and related drug-resistance issues. This is particularly relevant in targeted therapies where inhibition of the drug target can be overcome by cross-activating complementary pathways. Unfortunately, the drug combinations approved to date –mostly based on small molecules– face several problems such as toxicity effects, which limit their clinical use. To address these issues, we have designed a new class of RNase H-sensitive construct (3ASO) that can be disassembled intracellularly upon cell entry, leading to the simultaneous release of three different therapeutic oligonucleotides (ONs), tackling each of them the mRNA of a different protein. Here, we used *Escherichia coli* RNase H1 as a model to study an unprecedented mode of recognition and cleavage, that is mainly dictated by the topology of our RNA·DNA-based hybrid construct. As a model system for our technology we have created 3ASO constructs designed to specifically inhibit the expression of HER2, Akt and Hsp27 in HER2+ breast cancer cells. These trifunctional ON tools displayed very low toxicity and good levels of antiproliferative activity in HER2+ breast cancer cells. The present study will be of great potential in the fight against complex pathologies involving multiple mRNA targets, as the proposed cleavable designs will allow the efficient single-dose administration of different ON drugs simultaneously.

1. Introduction

Complex pathologies such as cancer or chronic inflammation are multi-factorial health conditions triggered by different factors acting together on an organism [1]. In the case of cancer, tumor progression is associated with a dynamic exchange of signals that interferes with multiple systems, including DNA repair, apoptotic and immune functions [2]. Plasticity of cancer networks is also responsible for many cases of acquired resistances to targeted therapies, which are characterized by activation of secondary signaling pathways of the tumor in response to perturbation of the major pathway, leading to cancer relapse [2,3]. As an example, Akt and Hsp27 are frequently overexpressed in HER2+ breast cancer, contributing to poor prognosis and drug resistance issues [4–8].

The most commonly used approaches to tackle complex disorders such as cancer and resistances rely on combination of small molecule drugs [9,10]. By using this strategy, therapies are more effective, reduce side effects and tackle cancer drug resistance targeting compensatory factors that can be already present or are activated in response to initial treatment. However, these treatments can face problems related to:

* Corresponding authors at: Department of Inorganic and Organic Chemistry, Organic Chemistry Section, Institute of Biomedicine, University of Barcelona (IBUB), Barcelona, Spain (M. Terrazas).
E-mail addresses: s.perez-torras@ub.edu (S. Pérez-Torras), montserrat.terrazas@ub.edu (M. Terrazas).
[1] Both authors contributed equally to this work.

https://doi.org/10.1016/j.bioorg.2024.107595
Received 8 May 2024; Received in revised form 13 June 2024; Accepted 24 June 2024
Available online 25 June 2024

difficulty to block relevant proteins because of the absence of well-defined binding pockets, toxicity effects linked to interaction of the drugs, and changes in bioavailability, metabolism and pharmacokinetic properties derived from combination of different drugs [9].

An alternative approach consists in the use of multifunctional conjugates composed of different ligands, each of them having its individual target [11–13]. Once exposed to intrinsic properties of the cells (i.e. enzymes or reducing agents), the multi-target molecule is disassembled, and its different drug components are released [11–13]. This strategy presents clear advantages with respect to conventional combined therapies, such as reduced drug dosage, reduced risk of drug interactions, a controlled induction of its multiple functions in the same cell, and more predictive pharmacokinetics. Such a design has been used in cell culture for the single-dose administration of small molecules of different characteristics, the majority of them based on Platinum or Ruthenium complexes, which trigger DNA damage [11–13].

A promising alternative can be the use of oligonucleotide (ON) molecules as drug components, specifically designed to bind the mRNAs that encode the disease-related proteins, thus inhibiting their expression with high selectivity [14–17]. ON therapeutics have received much attention in the last four decades due to their ability to inhibit the expression of virtually any gene in the human genome, thus allowing to approach proteins that cannot be targeted by small molecules. Among the different classes of therapeutic ONs that have been established, short interfering RNAs (siRNAs) [14–18] and antisense oligonucleotides (ASOs) [14–17,19] are amongst the most studied ones, due to their potency and selectivity. Over the past decade, most of the obstacles that face the clinical application of therapeutic ONs (i.e. nuclease degradation, poor cell uptake) have been overcome through the development of chemical modification approaches [i.e. replacement of one of the non-bridging oxygens of the phosphodiester linkage (PO) by a sulfur atom (phosphorothioate modification; PS) and 2′-*O*-Me, 2′-*O*-(2-methoxyethyl) substituents in the sugar ring] and delivery platforms [17]. Thanks to these approaches, significant progress has been achieved in the last ten years [14–17], with eighteen FDA-approved ONs currently in the market, all of them tackling a single target [16]. However, despite the great therapeutic potential of ONs, little research has been addressed to study their use in multi-target tools [20–32], with the majority of examples involving Dicer-induced [23,24,27,28] or reductive disulfide cleavage [26,29,31,32]. A limitation of Dicer-based constructs is that the ON drug precursors cannot bear biostable modifications near the scissile bonds, thus avoiding the co-delivery of fully modified siRNAs [33]. On the other hand, introduction of a disulfide linkage between two ON strands of different sequence is not a straightforward work and is mainly limited to two ON components [26].

Here, we present a novel RNase H-sensitive construct, 3ASO, based on a chimeric RNA DNA hybrid with two overhanging PS DNA strands, specifically designed for the simultaneous intracellular administration of three different fully-PS modified ASO drugs per dose (Fig. 1A). Making use of this technology, we have been able to simultaneously inhibit the expression of HER2, Akt and Hsp27 mRNAs in HER2+ breast cancer cells, achieving good levels of anti-proliferative activity and null toxicity in non-tumoral cells.

The nuclease-cleavable RNA·ASO (DNA) heteroduplex approach was first used by Yokota and co-workers to administer a single gapmer ASO with high efficiency and specificity [34–37]. The reported design (Fig. 1B) consists in a heteroduplex oligonucleotide (HDO) composed of the gapmer ASO and its complementary RNA conjugated to a lipid (α-tocopherol or cholesterol) and has been applied to inhibit gene expression in the liver [36], brain microvascular endothelial cells [34], the dorsal root ganglion and the sciatic nerve [37] in mice [34,35,37] and in non-human primates [36].

The promising results reported for the HDO heteroduplex reinforce the notion that ASO administration triggered by endogenous nucleases such as RNase H can be a breakthrough in the field of ON therapeutics and can open the door to many possibilities, such as multitargeting. Nevertheless, the RNase H-sensitive strategy has never been used to administer more than one ASO simultaneously. To our knowledge, the work reported here represents the first example of a multi-target ON tool with the ability to release multiple ONs of different sequence by RNase H activation.

RNase H enzymes are well known for their key role in key genetic processes, such as replication and transcription [38,39]. Additionally, RNase H recognition and function [40,41] have been exploited for therapeutic and biomedical/biotechnological purposes [42–51]. A very well-known and representative example is the RNase H-dependent ASO technology, that is based on recruitment of RNase H to degrade mRNA after ASO·RNA hybridization [19,42,43]. Other representative examples are nanomachines [50,51] –such as DNA-based rolling-motors [50]– powered by RNase H, RNase H-responsive nanoparticles for drug delivery [44], and hybrid siRNA-polyA-mRNA structures for enhancing anticancer T cell immunity [47], among others.

Due to its biological relevance, the structure and function of RNase H has received considerable attention [38–41]. Among the two types of RNase H enzymes that exist (RNase HI/HII in bacteria and RNase H1/H2 in eukaryotes) [38], RNase HI/H1 is found in many species, including

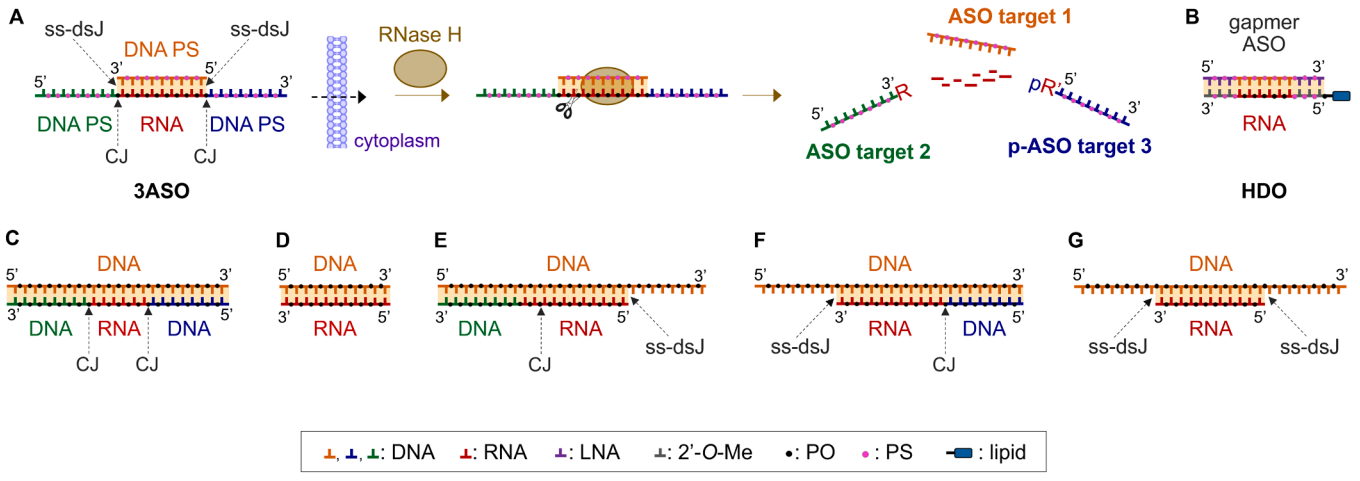

Fig. 1. (A) Representation of the 3ASO RNase H-sensitive approach for single-dose delivery of three different ASO analogues. (B) RNA·DNA heteroduplex (HDO) conjugate for the administration of a single gapmer ASO unit (LNA: locked nucleic acids; 2′-O-Me: 2′-O-methyl nucleosides) [34–37]. (C-G) Different RNA·DNA hybrid structures previously used in biochemical and structural RNase H studies [39,41,54–57].

viruses, bacteria and animals. *Escherichia coli* RNase HI is structurally very similar to the *C*-terminal catalytic domain of human RNase H1 [41]. For this reason, RNase HI has been intensively studied as a model of endonuclease that cleaves –via a two-metal ion catalysis– the RNA strand in RNA·DNA hybrids giving RNA-3′-OH and 5′-p-RNA fragments (p = phosphate) [52,53].

Up to date, several studies of RNase H recognition and cleavage activity of DNA·RNA hybrids have been performed, including: *i*) RNA·DNA hybrids flanked by two DNA duplexes (Fig. 1C) [39,54], *ii*) simple RNA·DNA hybrids (Fig. 1D) [41,55,56], *iii*) RNA·DNA hybrids flanked by a double-stranded (ds) DNA and a single-stranded (ss) 3′/5′-DNA overhang on the DNA side (Fig. 1E and F) [57], and *iv*) RNA·DNA hybrids flanked by two ssDNA overhangs on the DNA side (Fig. 1G) [57].

However, to our knowledge, nothing is known about the recognition and cleavage mode of RNA·DNA hybrids bearing ssDNA overhangs on the RNA side, i.e., as the ones contained in the 3ASO. Noteworthy, as an additional outcome of our study, we could elucidate an unprecedented mode of RNase H cleavage for this kind of ON architectures.

2. Results and discussion

2.1. Design and synthesis of 3ASO constructs

Our 3ASO design is based on a double-stranded construct composed of two building blocks: **ASO target 1** [top strand of the construct in Fig. 2A; fully PS-modified single-stranded (ss)DNA] and long chimeric ssON **L** (bottom strand of the construct in Fig. 2A). **L** is constituted by four different domains: *i*) fully PS-modified DNA (*A target 2* domain), *ii*) a bridge (*N*) consisting in a 2′-deoxyribonucleotide or a ribonucleotide, *iii*) an RNA stretch bearing PO linkages at all internucleotide positions (*B RNA* domain), *iv*) and fully PS-modified DNA (*C target 3* domain). The *B RNA* domain is connected to *N* and to the *C target 3* domain by PO linkages, while the *A target 2* domain is connected to *N* by a PS linkage. **ASO target 1** is complementary in sequence to the central RNA stretch (*B RNA* domain) of strand **L**, which is identical in sequence to a fragment of a mRNA encoding a specific protein. On the other hand, the *A target 2-N* stretch and the *C target 3* domain are identical in sequence to two ASOs targeting the mRNA of two other different proteins (**ASO target 2** and **ASO target 3**, respectively; Fig. 2).

We started our studies by synthesizing three 3ASO constructs targeting the HER2/Hsp27/Akt combination (constructs **1**–**3**; Fig. 2A), which were designed according to the following scheme: *i*) for 3ASO **1**, target 1, 2 and 3 are Hsp27, HER2 and Akt (length of the target sequences: 20 nt, 15 nt and 20 nt, respectively), and *N* = 2′-deoxynucleotide; *ii*) 3ASO **2** is a 3ASO **1** analogue (same sequences) with *N* = ribonucleotide [equivalent to displacement of the chimeric DNA–RNA joint (CJ) one nucleotide to the left, shortening the length of the ASO HER2 component to 14 nt], which was designed with the aim of investigating the effect of an extra 2′-OH group at the ds-ss junction (ss-dsJs) on RNase H recognition and cleavage; *iii*) for 3ASO **3**, target 1, 2 and 3 are HER2, Hsp27 and Akt (same sequences as before), respectively, and *N* = 2′-deoxynucleotide. A non-targeting, scrambled version of **3** (**4**) was also synthesized, as negative control for biological studies.

Formation of the branched constructs proceeded in a straightforward manner by combination of the two building blocks of each of the constructs (**ASO target 1** and long chimeric strand **L**, general scheme, Fig. 2A) under annealing conditions. As an example, analysis of the formation of 3ASO **1** by native PAGE (Fig. 2B) revealed a single product that migrated more slowly than each of its separated components (**ASO Hsp27** and **L1**). The same results were obtained for 3ASOs **2** and **3**, after combination of **ASO Hsp27** and **L2**, and **ASO HER2** and **L3**, respectively (Fig. 2B).

2.2. 3ASO recognition and cleavage by RNase H

To investigate the effect of two ss-dsJs and two chimeric DNA–RNA joints (CJ; Fig. 1A and 2A) on RNase H recognition and cleavage (where – stands for a PO linkage involved in a chimeric joint, and thus connecting a DNA and an RNA domain), 3ASO constructs **1**–**3** were incubated with RNase HI (from *Escherichia coli*) and the reactions were analyzed by native gel electrophoresis. For the analysis of each reaction, individual DNA PS ASO analogues of *A target 2-N* and *C target 3* domains [**ASO target 2** and **ASO Akt** (target 3 = Akt in all cases); Fig. 2A and 3B] were loaded as controls of potential products of cleavage at the *A target 2-N* (DNA)–*B RNA* (RNA) and at the *B RNA*–*C target 3* (DNA) CJs. Although cleavage at the *B RNA*–*C target 3* junction is expected to release 5′-phosphorylated **ASO target 3** (**p-ASO Akt**; Fig. 3A), non-phosphorylated **ASO Akt** was loaded as control due to lack of difference in electrophoretic mobility between these two ONs (see Fig. S1). Additionally, **ASO target 1** was also loaded as control in all cleavage reactions.

Promisingly, the 3ASO scaffold turned out to be a good substrate for

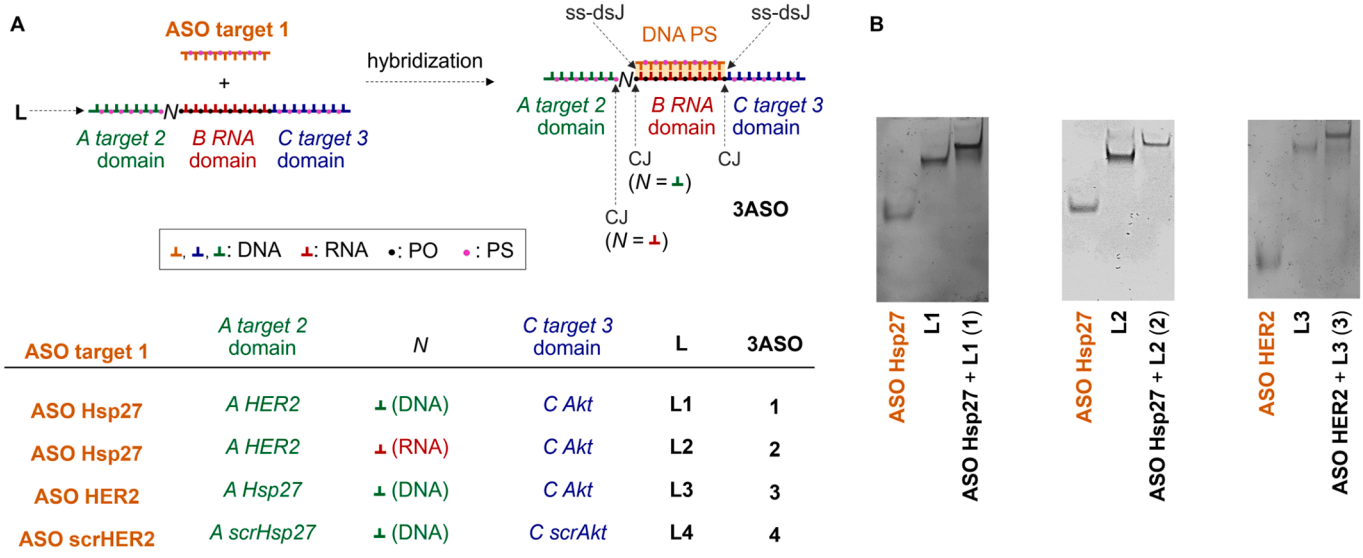

ASO target 1	A target 2 domain	N	C target 3 domain	L	3ASO
ASO Hsp27	A HER2	⊥ (DNA)	C Akt	L1	1
ASO Hsp27	A HER2	⊥ (RNA)	C Akt	L2	2
ASO HER2	A Hsp27	⊥ (DNA)	C Akt	L3	3
ASO scrHER2	A scrHsp27	⊥ (DNA)	C scrAkt	L4	4

Fig. 2. (A) Scheme of formation of the 3ASO construct. The composition of the different constructs used in this study is indicated (ss-dsJ = single-stranded-double-stranded junction; CJ = chimeric DNA–RNA joint). (B) Native PAGE analysis of the formation of 3ASO constructs **1**–**3**.

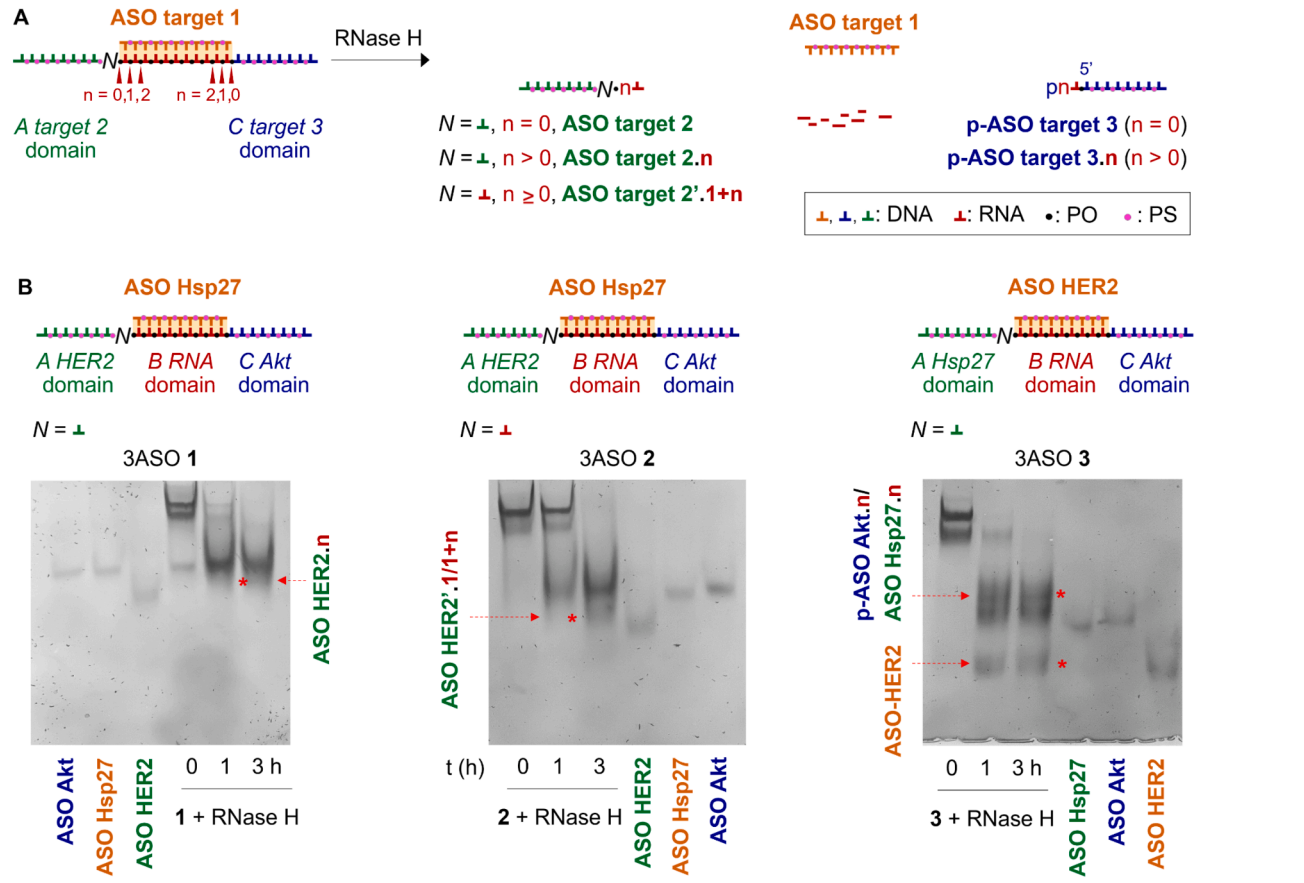

Fig. 3. (A) General scheme representing different possibilities of RNase H cleavage at DNA–RNA CJs and at PO RNA positions adjacent to the CJs. (B) Native PAGE analysis of RNase H cleavage reactions of 3ASO constructs **1**–**3** after phenol extraction, followed by ethanol precipitation. **ASO HER2′** = shorter version of **ASO HER2** missing one deoxynucleotide unit at the 3′ end.

RNase H, which completely digested constructs **1**–**3** in less than 1 h giving ON products with electrophoretic mobilities similar to those of the three independent ASOs (Fig. 3B). In the case of 3ASO **1**, a broad product band was observed, which migrated similarly to **ASO Hsp27** and to **ASO Akt** (which have similar electrophoretic mobilities). A very faint and smeared band that migrated slightly faster than the first product(s) and slower than **ASO HER2** was also detected, presumably corresponding to **ASO HER2** bearing a 3′-tail of 1 or 2 ribonucleotides a (**ASO HER2.n**; n = 1 or 2 ribonucleotides; Fig. 3A and B). Very similar results were obtained for ASO **2**, suggesting the release of its *A HER2-N* overhang with a short ribonucleotide tail attached to its 3′-end (presumably corresponding to **ASO HER2′.1** + **n**; **ASO HER2′** = shorter version of **ASO HER2** missing one deoxynucleotide unit at the 3′ end; n = 1 or 2; Fig. 3A and B). Additionally, a broad band of similar mobility to that of **ASO Akt** and **ASO Hsp27** was also observed. On the other hand, in the case of 3ASO **3**, a band of identical mobility to **ASO HER2** was detected, as well as a second one migrating similarly to **ASO Akt** and/or **ASO Hsp27**, and a third one of slightly lower mobility, probably corresponding to **ASO Akt** and/or **ASO Hsp27** bearing a short tail of ribonucleotides (**ASO Hsp27.n** and/or **ASO Akt.n**; Fig. 3A and B).

2.3. MALDI-TOF spectrometry analysis of RNase H-digested 3ASO constructs

To confirm the nature of the observed ON fragments, the three RNase H digestions were analyzed by MALDI-TOF mass spectrometry after 3 h of incubation (Fig. 4A, S2 and S3). In the case of the digested construct **1**, five main signals were detected in the mass range between 3000 and 10000, three of them [peaks at 6471.8 (broad and intense signal), 5079.3 and 5374.6 Da] corresponding to: *i*) **p-ASO Akt** and **ASO Hsp27** [broad signal at 6471.8 Da, presumably resulting from overlapping of **p-ASO Akt** and **ASO Hsp27** signals, of very similar masses (MWcalc = 6481.9 and 6477.3, respectively)], *ii*) **ASO HER 2** with an overhanging ribonucleotide (rA) attached to its 3′-end (ON fragment **ASO HER2.1**; Fig. 3A; see sequences of all ON fragments obtained from RNase H digestions in Table S2), and *iii*) **ASO HER 2** with a tail of two ribonucleotides (rApU) attached to its 3′-end (ON fragment **ASO HER2.2**), the first ON fragment (**p-ASO Akt**) originating from cleavage of the PO linkage covalently linking the central *B RNA* domain to *C Akt* DNA domain (*B RNA–C Akt* CJ), and the latter two (**ASO HER2.1** and **ASO HER2.2**) arising from cleavage of PO linkages positioned one and two base pairs (n = 1 and 2, respectively, in Fig. 3A and 4A) from the *N* bridge (a 2′-deoxyribonucleotide, in this case). Remarkably, ON fragments of masses larger than 6481.2 (calculated mass for **p-ASO Akt**) were not detected, thus ruling out the presence of ribonucleotide tails attached to **p-ASO Akt**. On the other hand, according to the mass spectrum, cleavage of the left arm of the construct takes place mainly at position n = 2, since the peak corresponding to **ASO HER2.2** (n = 2) was much more intense than that of **ASO HER2.1** (n = 1). The other two peaks (5238.0 and 6321.4; Fig. S2A) arose from MALDI-TOF induced depurination (loss of G nucleobase) of **ASO HER2.2** and **ASO Hsp27**, respectively. A tendency of oligodeoxyribonucleotides ions to fragment, dominated by loss of nucleobases (mainly G and A), has been reported in MALDI mass spectrometry of DNA molecules [58–61]. This process has been suggested to take place during the laser desorption/ionization process and is sequence-length dependent. Indeed, loss of G nucleobase was also detected in MALDI-TOF mass analysis of pure control ONs of the same sequence and composition as the cleavage products (see Table S1).

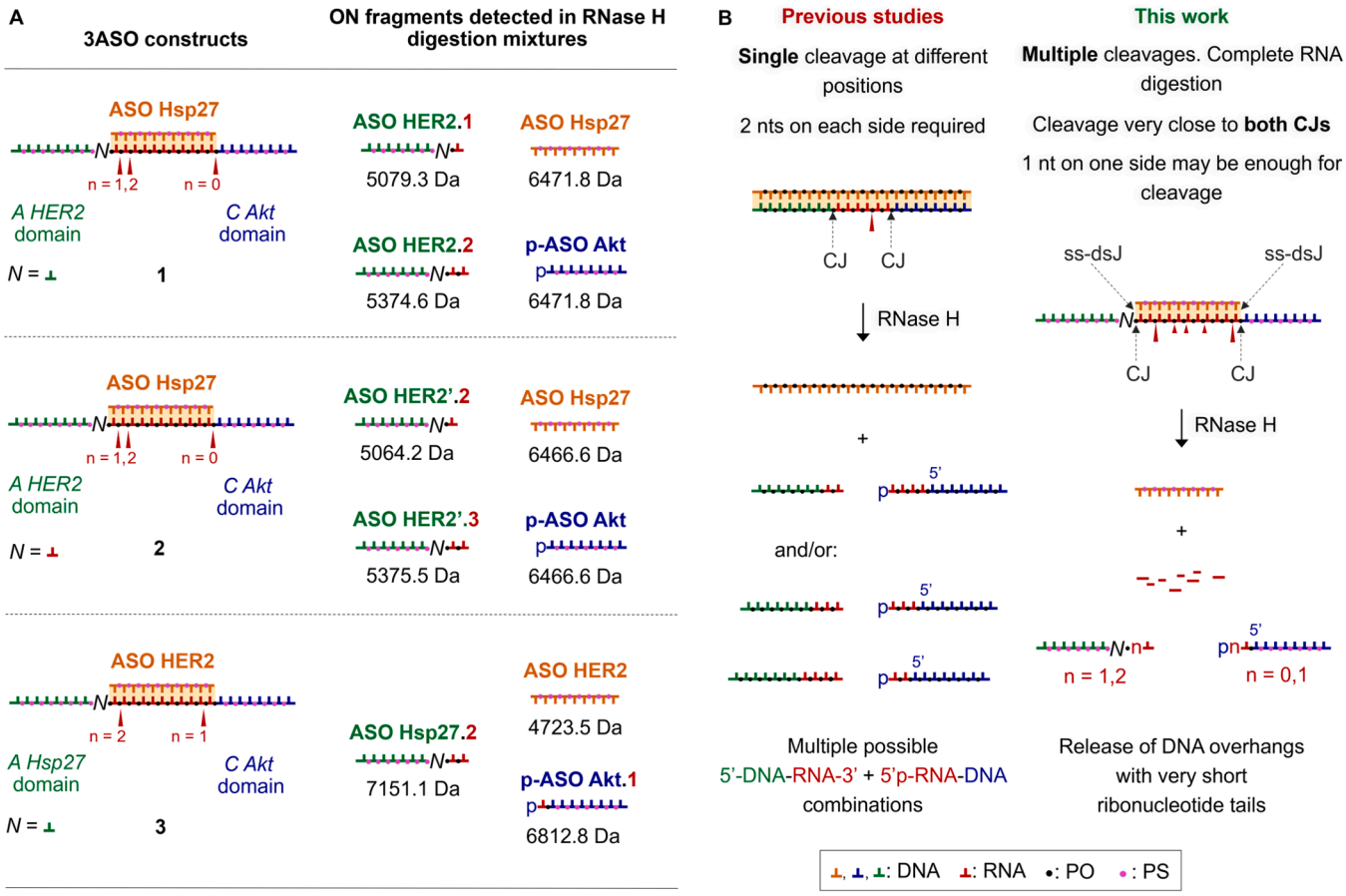

Fig. 4. (A) ON fragments detected by MALDI-TOF mass spectrometry after RNase H digestion of each 3ASO construct. Red arrowheads indicate the positions at which the RNase H cleaves the heteroduplex substrate. (B) A comparison between the mode of RNase H cleavage observed in our construct, bearing two CJs and two ssDNA overhangs on the RNA side, and that previously reported for DNA·RNA hybrids flanked by two dsDNAs [39,54], i.e. the only structures reported so far with two CJs. (For interpretation of the references to colour in this figure legend, the reader is referred to the web version of this article.)

In the case of the digested construct **2**, its mass spectrum revealed four peaks, the first two (at 5064.2 and 5375.5 Da) corresponding to two **ASO HER2′** derivatives bearing a 3′-tail of two and three ribonucleotides, respectively (rCpA and rCpApU tails; ON fragments **ASO HER2′.2** and **ASO HER2′.3**; Fig. 3A, 4A and S2B), arising from cleavage of the PO linkages positioned one and two base pairs (n = 1 and 2, respectively, in Fig. 4A) from the *N* bridge (in this case, a ribonucleotide). Interestingly, and in contrast to the results obtained for construct **1**, the product of cleavage at position n = 2 (**ASO HER2′.3**, Fig. 4A) was now barely detected in the mass spectrum (Fig. S2), being **ASO HER2′.2** (product of cleavage at position n = 1) the predominant one. Nevertheless, although displacement of the CJ to the left shifted the cleavage position one nt to the left, this was not translated in a decrease in length of the 3′-ribonucleotide tail. Similarly to what had been observed for construct **1**, a third and more intense peak at 6466.6 Da was also observed, presumably resulting from overlapping of **p-ASO Akt** and **ASO Hsp27** signals (MWcalc = 6481.9 and 6477.3, respectively).

Finally, the mass spectrum of the digested construct **3** revealed three main peaks at 4723.5, 6813.0 and 7151.1, corresponding to: *i*) **ASO HER2**, *ii*) **ASO Akt** with a 5′-phosphorylated ribonucleotide (prG) attached to its 5′-end (ON fragment **p-ASO Akt.1**), and *iii*) **ASO Hsp27** with a dinucleotide tail (rGpU) attached to its 3′-end (ON fragment **ASO Hsp27.2**), the second one arising from cleavage of the PO linkage one base pair from the nearest DNA residue of the overhanging *C Akt* domain (n = 1), and the third one arising from cleavage at position n = 2 from the *N* bridge (Fig. 3A, 4A and S2C). As before, a MALDI-TOF-induced depurination peak was detected (corresponding to a loss of guanine of **ASO Hsp27.2**; 6993.1 Da; Fig. S2C).

Importantly, in the three cases, analysis of the region of the mass spectra at mass over charge between 1000 and 3000 Da showed no peaks (Fig. S3), ruling out the formation of RNA fragments with length of four nucleotides or longer.

2.4. Comparison of 3ASO RNase H cleavage with that previously reported for other DNA·RNA hybrids

Our results suggest that RNase H recognizes both CJs and/or both ss-dsJs of our 3ASO design and cleaves very close to (or at) these positions –which is crucial to release the two overhanging ASOs practically clean–. Moreover, RNase H is cleaving sequentially at multiple points of the RNA strand, completely digesting it, probably into very small fragments (Fig. 4B).

To our knowledge, there are no reports on the RNase H recognition of RNA·DNA hybrids bearing two DNA-RNA CJs and two ssDNA overhangs on the RNA side, which corresponds to two ss-dsJs of the kind ssDNA–dsRNA·DNA (where – stands for a PO linkage involved in a chimeric joint, and thus connecting a DNA and an RNA domain, and · stands for Watson-Crick base pairing). Note that in our structures, the position of the CJs on the **L** strand coincides with that of the ss-dsJs, which is a topology that has not been investigated before. The only structures reported so far with two chimeric CJs are the RNA·DNA hybrids flanked by two DNA duplexes depicted in Fig. 1C. For this class of constructs, a single cleavage at different possible positions along the RNA stretch has been reported (Fig. 4B) [39,54], leading, as a

consequence, to the release of different pairs of DNA fragments with long RNA overhangs (5′-DNA–RNA-3′ + 5′-p-RNA–DNA) [54]. Similar results have been described for simple RNA·DNA hybrids lacking CJs (Fig. 1D) [41,55,56]. Additionally, it has been found that for these two classes of hybrids (Fig. 1C and D), a minimum of four ribonucleotides (two on each side of scissile PO linkage) is needed for RNase H cleavage.

On the other hand, the only chimeric constructs bearing ss–dsJs that have been reported so far are the ones reported by Lee et al. [57], consisting in RNA·DNA hybrids flanked by *i*) a dsDNA and a ss-3′/5′-DNA overhang on the DNA side (and, thus, bearing a CJ and a ss-dsJ of the kind ssDNA–dsDNA·RNA; Fig. 1E, F, respectively), and *ii*) two ssDNA overhangs on the DNA side (and thus lacking CJs and bearing two ss-dsJs of the kind ssDNA–dsDNA·RNA; Fig. 1G) [57]. In the case of 3′-overhang-bearing hybrids (Fig. 1E), the primary and the secondary RNase H binding site appears at the ss–dsJ and at the CJ, respectively, the former becoming more predominant as the length of the RNA·DNA portion decreases, which ultimately results in an exonuclease processive complete degradation facilitated by the 3′-overhang [57]. For the 5′-overhang-bearing hybrid (Fig. 1F), RNase H binds equally to both the CJ and ds–ssJ, resulting in an endonuclease distributive and non-specific incomplete degradation. Finally, for the last case (RNA·DNA hybrids flanked by two ssDNA overhangs on the DNA side; Fig. 1G), RNase H binds mainly the two ds–ssJs, with binding probability of the ss–dsJ on the 3′ side 3-fold higher than that on the ss–dsJ on the 5′-side [57].

Remarkably, the multiple cleavage and consequent delivery of **ASO target 2.n** and **ASO target 3.n** (n = 0, 1 or 2 ribonucleotide units; Fig. 3A and 4A) observed for our constructs are in clear contrast to the results reported for the first group of hybrids flanked by two DNA duplexes (Fig. 1C and 4B). Additionally, in our case, the presence of one ribonucleotide on each side of the scissile PO linkage is enough for RNase H cleavage (n = 1, Figs. 3 and 4), while in the literature, two nucleotides on each side are required (Fig. 4B) [39,41,54–56].

On the other hand, despite relevant structural/topology differences between our 3ASO scaffold and the reported ssDNA overhang-bearing constructs (Fig. 1E–G), both families of structures possess ds-ssJs. The main difference with our work is that the region of the duplex that is covalently connected to the ssDNA overhang is DNA (ssDNA–dsDNA·RNA joint) in the reported examples (Fig. 1E–G; versus a ssDNA–dsRNA·DNA joint, in our case). Additionally, the reported ssDNA overhang-bearing hybrids (Fig. 1E and F) share, in part, another structural feature with our constructs; namely, the presence of a CJ in their structure. Such subtle resemblances may account for the higher RNase H binding at these chimeric positions in our constructs. It is noteworthy that our results reveal binding of RNase H closer to the nearest DNA residue of the 3′-overhanging ssDNA than to the nearest DNA residue of the 5′-overhanging ssDNA (left and right of the construct, respectively), which could also be in agreement with the preference for 3′-overhang ss-dsJs observed for the reported hybrids (Fig. 1E and G) [57]. In particular, cleavage at the left side of the central RNA·DNA hybrid in constructs **1** and **3** gives **ASO HER2** and **ASO Hsp27** with a tail of two ribonucleotides attached to their 3′-end as main products, arising from scission of the PO linkage located two base pairs from the nearest DNA nucleotide residue of the unpaired *N* bridge (*N* = deoxynucleotide; n = 2; Figs. 3 and 4). On the other hand, cleavage at the right side of the hybrid component of the same constructs (**1** and **3**) led to the release of **ASO Akt** with a shorter ribonucleotide tail attached to its 5′-end. Specifically, a 5′-monoribonucleotide overhang for the case of **3** and no ribonucleotide tail for **1**, which also suggest sequence-dependence in the process of recognition and cleavage.

In addition to these observations, the results obtained for 3ASOs **1** and **2** further confirms that RNase H cleavage is not only dictated by the ss-ds junction of our constructs but by both chimeric RNA-DNA joints, as cleavage at the left side of the hybrid in construct **2**, bearing an unpaired ribonucleotide bridge between the ssDNA overhang and the central RNA stretch (*N*), gave mainly **ASO HER2′.2**, resulting from cleavage at only one base pair from the nearest nucleotide of the overhanging arm (*N*).

Altogether, our studies provide deeper insight into the effect of CJs and ss-dsJs on RNase H and cleavage, and gives support to the notion that RNase H mode of action is mainly dictated by these structural elements. Such structure–function relationships can be exploited to create hybrid structures with great biotechnological/therapeutic potential, such as the newly designed 3ASO, to allow the simultaneous release their multiple ON components, practically clean, upon RNase H recognition.

2.5. Ability of ASOs and 3ASO constructs to silence target genes

To investigate if our 3ASO designs can be processed by RNase H not only *in vitro*, but also inside the cell, we first verified the effectiveness of individual ASOs (**ASO Hsp27**, **ASO Akt** and **ASO HER2**) (Fig. 5). SK-BR-3 cells were transfected with the various ONs (20 nM), and Hsp27, HER2 and Akt expression levels were assessed by western blot 48 h and 72 h after transfection. **ASO Hsp27** and **ASO Akt** showed a time-dependent activity, whereas **ASO HER2** activity was only observed at 48 h. Inhibitory levels of Akt, Hsp27 and HER2 expression in cells treated separately with **ASO Akt**, **ASO Hsp27**, and **ASO HER2** were (45 ± 16)%, (46 ± 4)% and (53 ± 9)% on day 2, and (73 ± 8)%, (68 ± 7)% and 0 % on day 3. All the results were normalized to basal condition (Fig. 5).

Once proved the inhibitory effect of the individual ONs, we carried out the experiments with the two constructs bearing fully DNA PS-modified overhangs (*N* = deoxynucleotide; **1** and **3**) compared with non-targeting 3ASO **4** (Fig. 6). The only difference between 3ASO **1** and **3** is that their central domain and left arm domain are exchanged: 3ASO

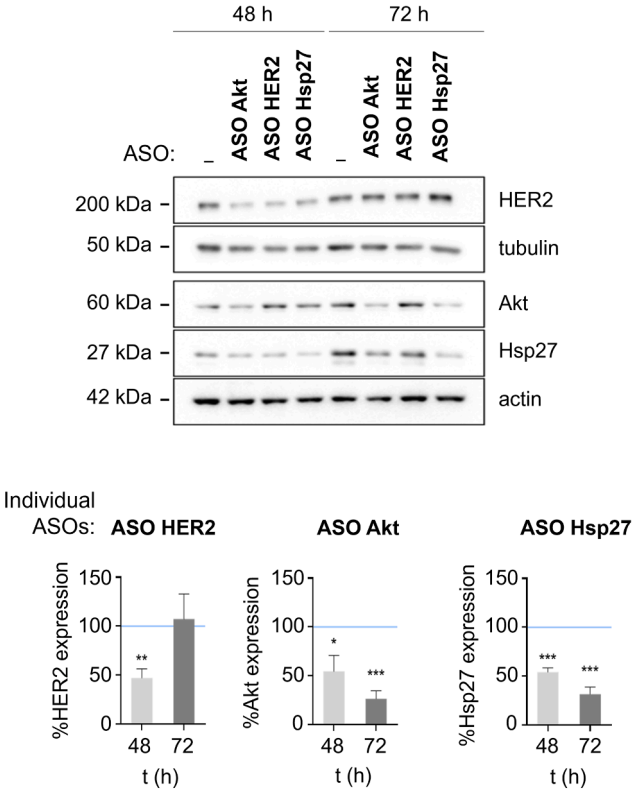

Fig. 5. Effectiveness of individual ONs. Representative immunoblots and quantitative analysis of protein expression for HER2, Akt, Hsp27, actin (internal control) and tubulin (internal control) from SK-BR-3 cells treated with individual ASOs (**ASO HER2**, **ASO Akt** and **ASO Hsp27**) and non-treated cells (– control). Three independent assays were performed and quantified. Results are expressed as means ± SEM (*p < 0.05, **p < 0.01, ***p < 0.005; unpaired Student's *t* test). The corresponding control is indicated with a horizontal line.

1 targeting HER2 at left arm and Hsp27 at the central part, while 3ASO **3** is the other way around (Fig. 6A). The position is relevant in terms of 3ASO-induced target reduction, displaying some significant differences. In particular, in the case of 3ASO **1**, the inhibition of HER2 is not effective, whereas Akt and Hsp27 proteins expression was (49 ± 5)% and (29 ± 22)% on day 2, and (50 ± 14)% and (63 ± 14)% on day 3, respectively, while the reduction of Akt, Hsp27 and HER2 protein levels for 3ASO **3** were (64 ± 3)%, (46 ± 10)% and (26 ± 13)% on day 2, and (60 ± 7)%, (61 ± 13)%, and (50 ± 5)% on day 3. These results reveal that a 20 nt DNA overhang at the left side of the construct (*A Hsp27-N* overhang) is better tolerated than a shorter one (15 nt; *A HER2-N* overhang), which could be related to the length of the ASO-specific recognition sequence. In this regard, **ASO Hsp27** activity appears to be less affected than that of **ASO HER2** by the presumable remaining tail of two ribonucleotides attached to their 3′-end after RNase H action when they are located at the left arm. Remarkably, the 15 nt HER2-targeting component displayed a stronger inhibitory effect when located in the central part of the construct and released in its free form, achieving longer duration of action than individual ASO HER2.

In a parallel experiment, SK-BR-3 cells were treated with 3ASO **2** [*A target 2-N* (left arm of the construct in Fig. 2) targeting HER2, *N* = ribonucleotide; **ASO target 1** component (central part of the construct) targeting Hsp27, and *C target 3* (right arm of the construct in Fig. 2) targeting Akt], leading to inhibitory levels of Akt and Hsp27 expression comparable to those obtained for construct **1** and detectable anti-HER2 activity. (Fig. S4).

Finally, to ensure the specificity of the observed effects, the same cell line was only treated with the long chimeric strand component of 3ASO construct (**L3**). Levels of the Akt protein remained practically unaffected (Fig. S5), contrary to what was observed with individual **ASO Akt**, 3ASO **1** and 3ASO **3**. These results clearly demonstrate that the inhibitory effect observed for the 3ASO constructs is strictly controlled by RNase H cleavage of the central RNA domain of the 3ASO construct and the consequent release of the three independent active ASOs, thus suggesting that the long *RNA −C target 2* and *A target 2-RNA* stretches of **L** may interfere with binding of *A target 2* domain and *C target 2* domain to their target mRNA counterparts, respectively, preventing their activity.

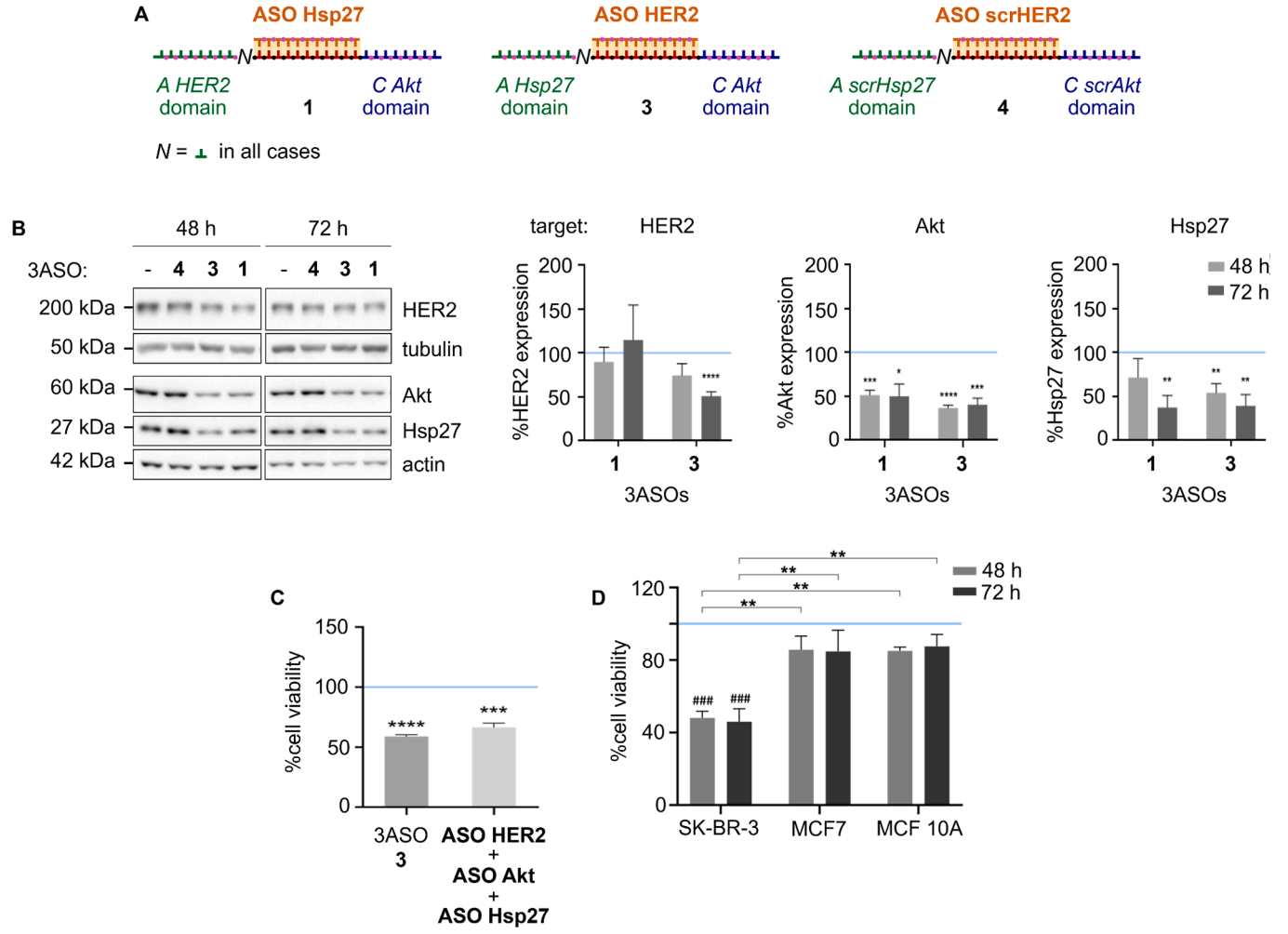

Fig. 6. Biological effect of 3ASO constructs. (A) Scheme of 3ASO constructs used in this study. (B) Representative immunoblots and quantitative analysis of protein expression for HER2, Akt, Hsp27, actin (internal control) and tubulin (internal control) from SK-BR-3 cells treated with 3ASO constructs **1**, **3** and **4**. (C) CCK8 viability assay 48 h after transfection of SK-BR-3 cells with 3ASOs **3** and **4** and with a 1:1:1 mixture of **ASO HER2**, **ASO Akt** and **ASO Hsp27**. (D) MTT viability assay after transfection of SK-BR-3, MCF7 and MCF 10A cells with 3ASOs **3** and **4**. All the results (B-D) were normalized with 3ASO **4**, that did not have any effect on the cell lines used in this study. Independent assays were performed and quantified (n = 4 for western blot and n = 3 for viability assays). Results are expressed as means ± SEM. For B and C, unpaired Student's *t* test was performed comparing each bar to its control, indicated with a horizontal line (*p < 0.05, **p < 0.01, ***p < 0.005, ****p < 0.001). For D, significance was assessed by 2-way ANOVA, comparing to the control (indicated above the bar; ###p < 0.005) and between groups (with square brackets; **p < 0.01).

2.6. Impact of ASOs and 3ASO constructs on cell viability

ASO-mediated silencing of Akt, Hsp27 and HER2 (independently) is known to decrease the viability of HER2+ breast cancer cells such as SK-BR-3 [62–64], with no effect on luminal A (ER/PR+/HER2-) MCF7 breast cancer cells [63]. To investigate the potential beneficial effect of the 3ASO-mediated knockdown of Akt/Hsp27/HER2 gene combination on breast cancer therapy, we carried out cell viability studies with our best 3ASO design (**3**) and a 1:1:1 mixture of the three individual ASOs (**ASO Akt**, **ASO Hsp27** and **ASO HER2**), quantified 48 h after transfection (Fig. 6C) using the CCK8 assay. Cell viability levels were referred to those of cells treated with scrambled 3ASO **4**, which did not have any effect on this cell line. The viability of SK-BR-3 transfected with **3** was significantly reduced, with a decrease in cell proliferation that tends to be even higher than that obtained in cells transfected with the mixture of the three individual ASOs (Fig. 6C), confirming the efficiency of our 3ASO co-delivery strategy.

Importantly, non-malignant MCF 10A breast epithelial cells and HER2 negative, luminal A MCF7 breast cancer cells were unaffected when treated with 3ASO **3** (Fig. 6D), confirming the specificity and the low toxicity of our 3ASO design.

Taken together, the results obtained from our cell culture experiments are in good agreement with the digestion pattern observed for *in vitro* RNase H cleavage (Fig. 3B, 4 and S2), suggesting that RNase H processing of our 3ASO construct can also take place inside the cell, simultaneously releasing the three active ASOs. Our *in vitro* experiments demonstrated RNase H cleavage of PO linkages located nearby to the two DNA-RNA joints of the **L** component of the construct, leading to the release of intact **ASO target 1** and the two overhanging ASOs (**ASO target 2** and **ASO target 3**) bearing a small tail of n ribonucleotides (n = 0–2) at their 3′ and 5′ ends, respectively (5′-phosphorylated, in the case of **ASO target 3**). Western blot analysis of cells treated with constructs **1** and **3** revealed that these short ribonucleotide overhangs do not interfere with the activity of ASOs of 20 nt in length (**ASO Hsp27** and **ASO Akt**). As an example, the 5′-phosphorylated ASO product arising from the cleavage of 3ASOs **1** and **2** (**p-ASO Akt**, lacking a 5′-ribonucleotide tail) displayed activities comparable to that of the 5′-phosphorylated ASO product of 3ASO **3** cleavage (**p-ASO Akt.1**; bearing a 1 nt-ribonucleotide tail at its 5′-end), as well as to that of **ASO Akt** in its free form. However, shorter ASOs (15 nt in length; i.e. **ASO HER2**) appeared to be more affected by a short ribonucleotide tail, according to the lack of activity observed for the ASO products arising from cleavage of the left arm of construct **1** (**ASO HER2.1** and **ASO HER2.2**; bearing 1 nt- and 2 nt-ribonucleotide tails at their 3′-end, respectively), and to the recovery in activity observed when the **ASO HER2** was released in its free form (in the case of RNase H digestion of 3ASO **3**). Thus, altogether, these results suggest that the location of the shorter ASO component of the 3ASO construct is crucial for its optimal performance, and that the optimal design corresponds to construct **3**, which accommodates this fragment in the middle. Additionally, this 3ASO construct tended to show a higher anti-proliferative activity than a 1:1:1 mixture of the three individual ASOs. This could be reasonably ascribed to the ability of our construct 3ASO to deliver simultaneously the three therapeutic ONs.

3. Conclusion

In summary, we have created a new class multitarget ON tool with great potential in the treatment of complex diseases that rely on the use of multiple drugs. Multidrug treatment requires the combination of drugs that often have different pharmacokinetic parameters and even different dosage schedules, which hamper the bioavailability at the target site. In this context, the codelivery of multiple drugs, including ASOs, in a specific cell may be challenging. Our 3ASO construct overcomes this limitation allowing the simultaneous administration of three different drugs after recognition by intracellular RNase H, that specifically cleaves the RNA strand of the internal RNA·DNA hybrid by an unprecedented mode of action. The topology of our construct promotes RNase H recognition of both chimeric DNA-RNA joints and ss-dsJs of the construct, followed by cleavage of PO linkages located nearby to these two positions, which is crucial to release the active ASOs practically clean. The best 3ASO design, corresponding to two overhanging DNA PS regions of 20 nts in length and a central 15 bp DNA·RNA hybrid, could be used for targeting the Hsp27/HER2/Akt combination in SK-BR-3 cells with longer duration of action and higher antiproliferative activity than a mixture of its three separate ASO components.

Altogether, the structural characteristics and biological properties of the 3ASO construct makes it a new class of RNase H substrates of particular interest for the design of future multi-functional agents for biomedical and biotechnological applications. Since the two overhanging ON fragments of the 3ASO construct are not involved in hybrid formation, they can be modified at will (for example allowing LNA and 2′-*O*-Me substitutions), thus enabling the delivery not only of ASOs acting as RNase H activators (fully DNA or gamper DNA/LNA), but also of splice-switching ASOs, and other therapeutic ONs. Additionally, the promising results reported for the HDO heteroduplex conjugates [34–37], together with the multivalent properties of our 3ASO approach open the door to a broad range of new possibilities. Among them, the possibility to functionalize the 3ASO construct for its *in vivo* application with a targeting ligand conjugated at the end of the two overhanging ASOs. In this sense, functionalization of ASOs at the 3′ or 5′ termini with ligands such as GalNac has been reported to be compatible with ASOs activity and to even improve efficacy [65]. Another possibility could consist in the implementation of the 3ASO strategy to different classes of drugs (small molecules, different types of therapeutic oligonucleotides…) and to multiple combination of targets and diseases, and the possibility to tackle unreachable proteins.

4. Methods

4.1. General experimental methods

Reagents for oligonucleotide synthesis including 5′-*O*-DMT-2′-*O*-TBDMS-protected phosphoramidite monomers of natural ribonucleotides (A^{Bz}, C^{Ac}, G^{dmf} and U), 5′-*O*-DMT-protected phosphoramidites of natural 2′-deoxynucleotides (dA^{Bz}, dC^{Ac}, dG^{dmf} and T), the 5′-deblocking solution (3 % TCA in CH_2Cl_2), activator (5-benzylthio-1-*H*-tetrazole), CAP a solution (acetic anhydride/pyridine/THF), CAP B solution (THF/*N*-methylimidazole 84/16), oxidizing solution (0.02 M iodine in tetrahydro-furan/pyridine/water (7:2:1)) and [(dimethylaminomethylidene)amino]–3*H*-1,2,4-dithiazole-3-thione (Sulfurizing Reagent II; DDTT), 5′-*O*-DMT-dA^{Bz}-3′-succinyl-LCAA-CPG, 5′-*O*-DMT-dC^{Ac}-3′-succinyl-LCAA-CPG, 5′-*O*-DMT-dG^{dmf}-3′-succinyl-LCAA-CPG, 5′-*O*-DMT-T-3′-succinyl-LCAA-CPG, 5′-*O*-DMT-rA^{Bz}-3′-succinyl-LCAA-CPG and 5′-*O*-DMT-rC^{Ac}-3′-succinyl-LCAA-CPG were purchased from biosearch Technologies (LGC, Teddington, Middlesex, UK). Phenol/Chloroform/Isoamyl alcohol (25:24:1; stabilized and saturated with 100 mM Tris-EDTA to pH 8.0) and RNase H (5 U/μL) were purchased from Fisher Scientific (Thermo Fisher Scientific Inc, Spain)

MALDI-TOF mass spectra were obtained using an Applied Biosystems 4800 MALDI-TOF/TOF instrument. The matrix used contained 2,4,6-trihydroxyacetophenone (THAP, 10 mg/mL in CH_3CN/water 1:1) and ammonium citrate (50 mg/mL in water).

4.2. Oligonucleotide synthesis

All sequences were synthesized at the 1 μmol scale via solid phase synthesis using standard phosphoramidite methods [66] and an automated K&A S-4-LC DNA/RNA synthesizer (K&A labs gmh; Shaafheim, Germany). For the synthesis of DNA PS ONs **ASO Hsp27**, **ASO Akt**, **ASO HER2**, **ASO scrHER2** and **ASO HER2′**, 5′-*O*-DMT-protected phosphoramidites of natural 2′-deoxynucleotides (dA^{Bz}, dC^{Ac}, dG^{dmf} and T) and 5′-*O*-DMT-T-3′-succinyl-LCAA-CPG, 5′-*O*-DMT-dG^{dmf}-3′-succinyl-LCAA-

CPG, 5′-*O*-DMT-dC^{Ac}-3′-succinyl-LCAA-CPG and 5′-*O*-DMT-dA^{Bz}-3′-succinyl-LCAA-CPG solid supports were used. The following solutions were employed: 0.3 M 5-benzylthio-1-*H*-tetrazole in CH_3CN (activator), CAP a solution (acetic anhydride/pyridine/THF), CAP B solution (THF/*N*-methylimidazole 84/16) and sulfurizing solution (0.05 M sulfurizing Reagent II in pyridine-acetonitrile 60:40). Coupling and sulfurizing times were 40 and 360 s, respectively. The synthesis of the long chimeric ON components of the 3ASO constructs (**L1-L4**; bottom strands in Fig. 2) was conducted in three steps: i) synthesis of the *C target 2* domain, DNA-PS (right arm of the construct in Fig. 2), by applying the same approach as the one used for the synthesis of DNA-PS ASOs; ii) its elongation, using 2′-*O*-TBDMS-protected phosphoramidites of natural ribonucleotides, a 0.02 M iodine in tetrahydro-furan/pyridine/water (7:2:1) solution as oxidizer, and a coupling time of 10 min [i.e. Synthesis of the central B RNA domain (and n bridge in the case of **L2**)]; iii) elongation of the central *B RNA* domain (*N* bridge-*B RNA* domain in the case of **L2**), using the same strategy as the one used for the synthesis of DNA-PS ASOs, with the exception of the coupling time, which was 10 min (i.e. Synthesis of the a target 2 domain; left arm of the construct in Fig. 2)

After solid-phase synthesis, DNA PS ONs **ASO Hsp27**, **ASO Akt**, **ASO HER2**, **ASO scrHER2** and **ASO HER2′** were cleaved from the solid support and deprotected by incubation with 1 mL of NH_3 solution (33 %) at 55 °C for 1 h in a screw-cap vial. The vial was then allowed to cool down to room temperature and the ONs were purified using Glen-Pack Cartridges (Glen Research; Sterling, VA, USA) according to manufacturer's instructions. Long chimeric ONs **L1-L4** were cleaved from the solid support and deprotected by incubation with 1.5 mL of NH_3 solution (33 %) and 0.5 mL of ethanol at 55 °C for 1 h in a screw-cap vial. The vial was then cooled on ice and the supernatant was transferred into a 2 mL Eppendorf tube. The solid support and vial were rinsed with 50 % ethanol (2 x 0.25 mL). The combined solutions were evaporated to dryness using an evaporating centrifuge. The residue that was obtained was dissolved in DMSO (115 μL). After addition of 60 μL of triethylamine and 75 μL of triethylamine trihydrofloride, the resulting solution was incubated at 65 °C for 2.5 h. Then, the oligonucleotides were purified using Glen-Pack Cartridges according to manufacturer's instructions. The oligonucleotides were then purified by 20 % polyacrylamide gel electrophoresis (DMT-OFF). After purification, the ONs were isolated by the crush and soak method, dialyzed, quantified by absorption at 260 nm and confirmed by MALDI mass spectrometry (see Table S1).

4.3. Construction of 3ASO constructs

For the construction of 3ASO constructs, equal amounts of a 60 μM solution of the long chimeric ON component (bottom strand in Fig. 2), a 60 μM solution of **ASO target 2** (top strand in Fig. 2), and 3X HEPES buffer (300 mM KOAc, 90 mM HEPES-KOH at pH 7.4, 6 mM magnesium acetate) were mixed together in an eppendorf tube. The resulting solution was heated for 3 min at 95 °C followed by 1 h at 37 °C and 15 h at 4 °C.

4.4. RNase H cleavage reactions of 3ASO hybrid duplexes

–Direct visualization of the reaction mixtures by PAGE. 3ASO constructs (20 μM) were mixed with RNase H enzyme (0.0062 U/μL) in 20 mM Tris·HCl, 40 mM KCl, 8 mM $MgCl_2$, 1 mM DTT, and 0.03 mg/mL BSA (pH 8.3) buffer. The mixtures were incubated at 37 °C. At appropriate times (0, 1 and 3 h), aliquots of the reaction mixture (16.7 μL; 6.6 pmol) were separated and added to a glycerol loading solution (3.3 μL), and the samples were run on a 15 % non-denaturing PAGE at 100 V and 4 °C for 7 h, using TBM running buffer containing 89 mM Tris, 89 mM boric acid and 1 mM $MgCl_2$. The gels were visualized with SYBR Gold (Invitrogen; Thermo Fisher Scientific Inc, Spain) using a Dual LED blue/white light transilluminator (Invitrogen; Thermo Fisher Scientific Inc, Spain).

–Analysis of RNase H reactions (free of protein ON extracts) by PAGE and MALDI TOF mass spectrometry.* 60 pmoles of each 3ASO construct were incubated in two separate vials with RNase H (0.0062 U/μL) for 1 and 3 h at 37 °C using the same conditions as before (final 3ASO concentration in each vial = 0.6 μM). The ON products were then isolated by phenol extraction (pH 8) followed by ethanol precipitation. In a third vial (corresponding to t = 0), the same procedure was performed, with the only difference that phenol was added immediately after addition of RNase H to the vial containing the 3ASO construct. Each of the ON pellets obtained after ethanol precipitation, were resuspended in 20 μL of water. 6.7 μL of each of the resulting ON solution (20 pmol ON) were mixed with 3.3 μL of glycerol loading buffer and subsequently loaded onto the gel (identical conditions as before). The remaining ON solution (40 pmol), corresponding to time point t = 3 h, was subjected to MALDI TOF mass spectrometry analysis.

*Phenol extraction and ethanol precipitation of the digested products was performed to improve band resolution. It is noteworthy that the digestion profiles obtained using this approach (Fig. 3B) were identical to those obtained by loading the RNase H digestions directly onto the gel (see Fig. S6).

4.5. Cell culture

SK-BR-3 (HTB-30™), MCF7 (HTB-22™) and MCF 10A (CRL-10317™) were obtained from ATCC (Promochem Partnership, Manassas, VA, USA), and grown in a monolayer on solid support at 37 °C in a humidified 5 % CO_2 atmosphere. SK-BR-3 were maintained in DMEM-F12 (1:1) (Life Technologies, Carlsbad, CA, USA) supplemented with 10 % inactivated fetal bovine serum (iFBS), 20 U/mL penicillin, and 20 μg/mL streptomycin (Life Technologies). MCF7 were maintained in DMEM (Life Technologies) supplemented with 10 % fetal bovine serum (FBS), 20 U/mL penicillin, and 20 μg/mL streptomycin. MCF 10A were maintained in DMEM-F12 (1:1) supplemented with 5 % iFBS, 20 U/mL penicillin, 20 μg/mL streptomycin, 100 ng/mL cholera toxin (Sigma-Aldrich, St. Louis, MO, USA), 10 μg/mL human insulin (Sigma-Aldrich), 12.5 ng/mL EGF (Thermo Fisher Scientific, Waltham, MA, USA), and 250 μg/mL hydrocortisone (Sigma-Aldrich). Both cell lines were confirmed to be mycoplasma free every 2 weeks by PCR amplification.

4.6. Transient transfection

For protein measurements, SK-BR-3 and MCF 10A were seeded in 6 multi-well plates at a cell density of 250,000 and 200,000 cell/well, respectively. For cell viability assays, SK-BR-3 were seeded at 10,000 cell/well density, whereas MCF7 and MCF 10A cells at 8,000, in 96-well plates with quintuplicates for every condition. In all cases, 24 h after seeding, cells were transfected with 20 nM of each 3ASO, ASO, or ASO combination using Lipofectamine 2000 (Thermo Fisher Scientific) for SK-BR-3 and MCF 10A, and Lipofectamine 3000 (Thermo Fisher Scientific) for MCF7, according to the manufacturer's instructions, during the indicated times of each experiment.

4.7. Western blot analysis

Whole-cell extracts were obtained with lysis buffer (20 mM Tris–HCl pH 8.0, 150 mM NaCl, 10 mM EDTA, 10 mM $Na_4P_2O_7$, 2 mM Na_3VO_4, 100 mM NaF, 1 mM β-glycerophosphate, 1 % Igepal CA-630) containing 1 % Complete Mini protease inhibitors (Roche, Mannheim, Germany) and 1 % phosphatase inhibitors cocktail (PhosSTOP, Roche). Protein concentration was determined by Bradford assay (Bio-rad, Hercules, CA, USA). 10–20 μg of protein of cell lysates were resolved by sodium dodecyl sulfate–polyacrylamide gel electrophoresis (SDS-PAGE) on 8 % or 12 % gels, and transferred to polyvinylidene difluoride (PVDF) membranes using standard methods. Membranes were immunoblotted with the indicated primary and secondary antibodies. A chemiluminescence detection kit (Thermo Fisher Scientific) was used to detect antibody labeling in iBright™ CL1500 Imaging System (Thermo Fisher Scientific), and the detected bands were quantified using iBright

analysis software (Thermo Fisher Scientific).

4.8. Antibodies

Akt antibody (sc1618) was purchased from Santa Cruz Biotechnology (Dallas, TE, USA), Hsp27 antibody (ab5579) was obtained from Abcam (Cambridge, UK), HER2 antibody (#2242) was purchased from Cell Signaling (Danvers, MA, USA), actin and tubulin antibodies were obtained from Sigma-Aldrich (A2066 and T6074, respectively). The corresponding horseradish peroxidase (HRP)-conjugated secondary antibodies were obtained from DakoCytomation (Glostrup, Denmark) and BioRad (Hercules, CA, USA). No-Stain™ Protein Labeling Reagent was used as an additional internal control (A44717, Invitrogen, Thermo Fisher Scientific).

4.9. Cell viability assays

After 48 h, CCK8 colorimetric assay (Sigma-Aldrich) was performed according to the manufacturer's protocol. After 48 or 72 h, MTT (3-[4,5-dimethylthiazol-2-yl]-2,5 diphenyl tetrazolium bromide; Sigma-Aldrich) was added to evaluate the cell viability by colorimetric assay. In both cases, cell survival was calculated considering the 100 % viability of the cells transfected with the control 3ASO **4**.

4.10. Statistical analysis

Western blot quantifications and CCK8 assays were analyzed with unpaired Student's *t* test, and MTT survival assay with two-way analysis of variance (ANOVA) using a post hoc Tukey test. All analyses were performed using GraphPad Prism (La Jolla, CA, USA). Differences were considered significant when $p < 0.05$ in all cases.

CRediT authorship contribution statement

Aida Mata-Ventosa: Writing – review & editing, Validation, Methodology, Investigation, Formal analysis. **Ariadna Vila-Planas:** Writing – review & editing, Validation, Methodology, Investigation, Formal analysis. **Aina Solsona-Pujol:** Methodology, Investigation. **Jordi de la Dueña:** Methodology, Investigation. **Maria Torrents:** Methodology, Investigation. **Eduardo Izquierdo-García:** Investigation. **Marçal Pastor-Anglada:** Writing – review & editing, Supervision, Resources, Investigation, Funding acquisition, Formal analysis, Conceptualization. **Sandra Pérez-Torras:** Writing – review & editing, Supervision, Resources, Methodology, Investigation, Funding acquisition, Formal analysis, Conceptualization. **Montserrat Terrazas:** Writing – review & editing, Writing – original draft, Supervision, Resources, Methodology, Investigation, Funding acquisition, Formal analysis, Conceptualization.

Declaration of competing interest

The authors declare that they have no known competing financial interests or personal relationships that could have appeared to influence the work reported in this paper.

Acknowledgements

This work was supported by the Instituto de Salud Carlos III (PI18/01964 to M.T.) and grant PID2021-124765OB-I00 funded by MCIN/AEI/ 10.13039/501100011033 and by "FEDER A way of making Europe" to SPT and MPA. CIBER is an initiative of Instituto de Salud Carlos III. We thank the mass spectrometry unit of the Faculty of Chemistry (University of Barcelona; CCiTUB) for data acquisition and technical support.

Appendix A. Supplementary data

Supplementary data to this article can be found online at https://doi.org/10.1016/j.bioorg.2024.107595.

References

[1] A. Talevi, Multi-target pharmacology: possibilities and limitations of the "skeleton key approach" from a medicinal chemist perspective, Front. Pharmacol. 6 (2015), https://doi.org/10.3389/fphar.2015.00205.
[2] D. Hanahan, Hallmarks of cancer: new dimensions, Cancer Discov. 12 (2022) 31–46, https://doi.org/10.1158/2159-8290.CD-21-1059.
[3] C. Holohan, S. Van Schaeybroeck, D.B. Longley, P.G. Johnston, Cancer drug resistance: an evolving paradigm, Nat. Rev. Cancer 13 (2013) 714–726, https://doi.org/10.1038/nrc3599.
[4] S.S. Bacus, D.A. Altomare, L. Lyass, D.M. Chin, M.P. Farrell, K. Gurova, A. Gudkov, J.R. Testa, AKT2 is frequently upregulated in HER-2/neu-positive breast cancers and may contribute to tumor aggressiveness by enhancing cell survival, Oncogene 21 (2002) 3532–3540, https://doi.org/10.1038/sj.onc.1205438.
[5] L. Wei, T.-T. Liu, H.-H. Wang, H.-M. Hong, A.L. Yu, H.-P. Feng, W.-W. Chang, Hsp27 participates in the maintenance of breast cancer stem cells through regulation of epithelial- mesenchymal transition and nuclear factor-B, Breast Cancer Res. 13 (2011) 1–13. http://breast-cancer-research.com/content/13/5/R101.
[6] Y. Zhuang, F. Zhang, Y. Xu, L. He, W. Huang, C. Hong, Y. Cui, Evaluating the expression of heat shock protein 27 and topoisomerase II α in a retrospective cohort of patients diagnosed with locally advanced breast cancer and treated with neoadjuvant anthracycline-based chemotherapies, Front. Oncol. 13 (2023) 1067179, https://doi.org/10.3389/fonc.2023.1067179.
[7] G. Alberti, G. Vergilio, L. Paladino, R. Barone, F. Cappello, E. Conway De Macario, A.J.L. Macario, F. Bucchieri, F. Rappa, The chaperone system in breast cancer: roles and therapeutic prospects of the molecular chaperones Hsp27, Hsp60, Hsp70, and Hsp 90, Int. J. Mol. Sci. 23 (2022) 7792, https://doi.org/10.3390/ijms23147792.
[8] E. Tokunaga, Y. Kimura, E. Oki, N. Ueda, M. Futatsugi, K. Mashino, M. Yamamoto, M. Ikebe, Y. Kakeji, H. Baba, Y. Maehara, Akt is frequently activated in HER2/neu-positive breast cancers and associated with poor prognosis among hormone-treated patients, Int. J. Cancer 118 (2006) 284–289, https://doi.org/10.1002/ijc.21358.
[9] K.C. Bulusu, R. Guha, D.J. Mason, R.P.I. Lewis, E. Muratov, Y. Kalantar Motamedi, M. Cokol, A. Bender, Modelling of compound combination effects and applications to efficacy and toxicity: state-of-the-art, challenges and perspectives, Drug Discov. Today 21 (2016) 225–238, https://doi.org/10.1016/j.drudis.2015.09.003.
[10] B. Al-Lazikani, U. Banerji, P. Workman, Combinatorial drug therapy for cancer in the post-genomic era, Nat. Biotechnol. 30 (2012) 679–692, https://doi.org/10.1038/nbt.2284.
[11] X. Wang, X. Wang, S. Jin, N. Muhammad, Z. Guo, Stimuli-responsive therapeutic metallodrugs, Chem. Rev. 119 (2019) 1138–1192, https://doi.org/10.1021/acs.chemrev.8b00209.
[12] R. Jia, L. Teng, L. Gao, T. Su, L. Fu, Z. Qiu, Y. Bi, Advances in multiple stimuli-responsive drug-delivery systems for cancer therapy, Int. J. Nanomedicine 16 (2021) 1525–1551, https://doi.org/10.2147/IJN.S293427.
[13] K. Suntharalingam, Y. Song, S.J. Lippard, Conjugation of vitamin E analog α-TOS to Pt(IV) complexes for dual-targeting anticancer therapy, Chem. Commun. 50 (2014) 2465–2468, https://doi.org/10.1039/c3cc48740g.
[14] A. Khvorova, J.K. Watts, The chemical evolution of oligonucleotide therapies of clinical utility, Nat. Biotechnol. 35 (2017) 238–248, https://doi.org/10.1038/nbt.3765.
[15] S. Thakur, A. Sinhari, P. Jain, H.R. Jadhav, A perspective on oligonucleotide therapy: approaches to patient customization, Front. Pharmacol. 13 (2022) 1006304, https://doi.org/10.3389/fphar.2022.1006304.
[16] M. Egli, M. Manoharan, Chemistry, structure and function of approved oligonucleotide therapeutics, Nucleic Acids Res. 51 (2023) 2529–2573, https://doi.org/10.1093/nar/gkad067.
[17] T.C. Roberts, R. Langer, M.J.A. Wood, Advances in oligonucleotide drug delivery, Nat. Rev. Drug Discov. 19 (2020) 673–694, https://doi.org/10.1038/s41573-020-0075-7.
[18] A. Fire, S. Xu, M.K. Montgomery, S.A. Kostas, S.E. Driver, C.C. Mello, Potent and specific genetic interference by double-stranded RNA in *Caenorhabditis elegans*, Nature 391 (1998) 806–811, https://doi.org/10.1038/35888.
[19] C. Rinaldi, M.J.A. Wood, Antisense oligonucleotides: the next frontier for treatment of neurological disorders, Nat. Rev. Neurol. 14 (2018) 9–21, https://doi.org/10.1038/nrneurol.2017.148.
[20] A. Goga, M. Stoffel, Therapeutic RNA-silencing oligonucleotides in metabolic diseases, Nat. Rev. Drug Discov. 21 (2022) 417–439, https://doi.org/10.1038/s41573-022-00407-5.
[21] M. Rubenstein, P. Tsui, P. Guinan, Combination chemotherapy employing bispecific antisense oligonucleotides having binding sites directed against an autocrine regulated growth pathway and bcl-2 for the treatment of prostate tumors, Med. Oncol. 24 (2007) 372–378, https://doi.org/10.1007/s12032-007-0023-y.
[22] D. Shu, Y. Shu, F. Haque, S. Abdelmawla, P. Guo, Thermodynamically stable RNA three-way junction for constructing multifunctional nanoparticles for delivery of therapeutics, Nat. Nanotechnol. 6 (2011) 658–667, https://doi.org/10.1038/nnano.2011.105.

[23] Y. Nakashima, H. Abe, N. Abe, K. Aikawa, Y. Ito, Branched RNA nanostructures for RNA interference, Chem. Commun. 47 (2011) 8367–8369, https://doi.org/10.1039/c1cc11780g.

[24] P. Tarapore, Y. Shu, P. Guo, S.-M. Ho, Application of Phi29 motor pRNA for targeted therapeutic delivery of siRNA silencing metallothionein-IIA and survivin in ovarian cancers, Mol. Ther. 19 (2011) 386–394, https://doi.org/10.1038/mt.2010.243.

[25] M. Rubenstein, K.M. Anderson, P. Tsui, P. Guinan, Synthesis of branched antisense oligonucleotides having multiple specificities: treatment of hormone insensitive prostate cancer, Med. Hypotheses 67 (2006) 1375–1380, https://doi.org/10.1016/j.mehy.2006.05.055.

[26] H.J. Chung, C.A. Hong, S.H. Lee, S.D. Jo, T.G. Park, Reducible siRNA dimeric conjugates for efficient cellular uptake and gene silencing, Bioconjug. Chem. 22 (2011) 299–306, https://doi.org/10.1021/bc100438m.

[27] D. Jasinski, F. Haque, D.W. Binzel, P. Guo, Advancement of the emerging field of RNA nanotechnology, ACS Nano 11 (2017) 1142–1164, https://doi.org/10.1021/acsnano.6b05737.

[28] M. Terrazas, D. Sánchez, F. Battistini, N. Villegas, I. Brun-Heath, M. Orozco, A multifunctional toolkit for target-directed cancer therapy, Chem. Commun. 55 (2019) 802–805, https://doi.org/10.1039/C8CC08823C.

[29] M. Endo, T. Majima, Control of a double helix DNA assembly by use of cross-linked oligonucleotides, J. Am. Chem. Soc. 125 (2003) 13654–13655, https://doi.org/10.1021/ja036752l.

[30] H. Lee, A.K.R. Lytton-Jean, Y. Chen, K.T. Love, A.I. Park, E.D. Karagiannis, A. Sehgal, W. Querbes, C.S. Zurenko, M. Jayaraman, C.G. Peng, K. Charisse, A. Borodovsky, M. Manoharan, J.S. Donahoe, J. Truelove, M. Nahrendorf, R. Langer, D.G. Anderson, Molecularly self-assembled nucleic acid nanoparticles for targeted in vivo siRNA delivery, Nat. Nanotechnol. 7 (2012) 389–393, https://doi.org/10.1038/nnano.2012.73.

[31] J. Li, C. Zheng, S. Cansiz, C. Wu, J. Xu, C. Cui, Y. Liu, W. Hou, Y. Wang, L. Zhang, I. Teng, H.-H. Yang, W. Tan, Self-assembly of DNA nanohydrogels with controllable size and stimuli-responsive property for targeted gene regulation therapy, J. Am. Chem. Soc. 137 (2015) 1412–1415, https://doi.org/10.1021/ja512293f.

[32] Y. Dong, C. Yao, Y. Zhu, L. Yang, D. Luo, D. Yang, DNA functional materials assembled from branched DNA: design, synthesis, and applications, Chem. Rev. 120 (2020) 9420–9481, https://doi.org/10.1021/acs.chemrev.0c00294.

[33] L.J. Bergeron, J.-P. Perreault, S.A. Elela, Short RNA duplexes guide sequence-dependent cleavage by human Dicer, RNA 16 (2010) 2464–2473, https://doi.org/10.1261/rna.2346510.

[34] H. Kuwahara, J. Song, T. Shimoura, K. Yoshida-Tanaka, T. Mizuno, T. Mochizuki, S. Zeniya, F. Li, K. Nishina, T. Nagata, S. Ito, H. Kusuhara, T. Yokota, Modulation of blood-brain barrier function by a heteroduplex oligonucleotide in vivo, Sci. Rep. 8 (2018) 4377, https://doi.org/10.1038/s41598-018-22577-2.

[35] T. Nagata, C.A. Dwyer, K. Yoshida-Tanaka, K. Ihara, M. Ohyagi, H. Kaburagi, H. Miyata, S. Ebihara, K. Yoshioka, T. Ishii, K. Miyata, K. Miyata, B. Powers, T. Igari, S. Yamamoto, N. Arimura, H. Hirabayashi, T. Uchihara, R.I. Hara, T. Wada, C.F. Bennett, P.P. Seth, F. Rigo, T. Yokota, Cholesterol-functionalized DNA/RNA heteroduplexes cross the blood–brain barrier and knock down genes in the rodent CNS, Nat. Biotechnol. 39 (2021) 1529–1536, https://doi.org/10.1038/s41587-021-00972-x.

[36] K. Nishina, W. Piao, K. Yoshida-Tanaka, Y. Sujino, T. Nishina, T. Yamamoto, K. Nitta, K. Yoshioka, H. Kuwahara, H. Yasuhara, T. Baba, F. Ono, K. Miyata, K. Miyake, P.P. Seth, A. Low, M. Yoshida, C.F. Bennett, K. Kataoka, H. Mizusawa, S. Obika, T. Yokota, DNA/RNA heteroduplex oligonucleotide for highly efficient gene silencing, Nat. Commun. 6 (2015) 7969, https://doi.org/10.1038/ncomms8969.

[37] H. Kaburagi, T. Nagata, M. Enomoto, T. Hirai, M. Ohyagi, K. Ihara, K. Yoshida-Tanaka, S. Ebihara, K. Asada, H. Yokoyama, A. Okawa, T. Yokota, Systemic DNA/RNA heteroduplex oligonucleotide administration for regulating the gene expression of dorsal root ganglion and sciatic nerve, Mol. Ther. - Nucleic Acids 28 (2022) 910–919, https://doi.org/10.1016/j.omtn.2022.05.006.

[38] M. Hyjek, M. Figiel, M. Nowotny, RNases H: structure and mechanism, DNA Repair 84 (2019) 102672, https://doi.org/10.1016/j.dnarep.2019.102672.

[39] S.M. Cerritelli, R.J. Crouch, Ribonuclease H: the enzymes in eukaryotes, FEBS J. 276 (2009) 1494–1505, https://doi.org/10.1111/j.1742-4658.2009.06908.x.

[40] S.J. Schultz, J.J. Champoux, RNase H activity: structure, specificity, and function in reverse transcription, Virus Res. 134 (2008) 86–103, https://doi.org/10.1016/j.virusres.2007.12.007.

[41] M. Nowotny, S.A. Gaidamakov, R. Ghirlando, S.M. Cerritelli, R.J. Crouch, W. Yang, Structure of human RNase H1 complexed with an RNA/DNA hybrid: insight into HIV reverse transcription, Mol. Cell 28 (2007) 264–276, https://doi.org/10.1016/j.molcel.2007.08.015.

[42] A.L.M.A. Ten Asbroek, M. Van Groenigen, M. Nooij, F. Baas, The involvement of human ribonucleases H1 and H2 in the variation of response of cells to antisense phosphorothioate oligonucleotides, Eur. J. Biochem. 269 (2002) 583–592, https://doi.org/10.1046/j.0014-2956.2001.02686.x.

[43] H. Wu, W.F. Lima, H. Zhang, A. Fan, H. Sun, S.T. Crooke, Determination of the role of the human RNase H1 in the pharmacology of DNA-like antisense drugs, J. Biol. Chem. 279 (2004) 17181–17189, https://doi.org/10.1074/jbc.M311683200.

[44] J. Liu, X. Lu, T. Wu, X. Wu, L. Han, B. Ding, Branched antisense and siRNA co-assembled nanoplatform for combined gene silencing and tumor therapy, Angew. Chem. Int. Ed. 60 (2021) 1853–1860, https://doi.org/10.1002/anie.202011174.

[45] F. Ding, Q. Mou, Y. Ma, G. Pan, Y. Guo, G. Tong, C.H.J. Choi, X. Zhu, C. Zhang, A crosslinked nucleic acid nanogel for effective siRNA delivery and antitumor therapy, Angew. Chem. Int. Ed. 57 (2018) 3064–3068, https://doi.org/10.1002/anie.201711242.

[46] A.R. Chandrasekaran, R. Trivedi, K. Halvorsen, Ribonuclease-responsive DNA nanoswitches, Cell Rep. Phys. Sci. 1 (2020) 100117, https://doi.org/10.1016/j.xcrp.2020.100117.

[47] K. Lee, T.-S. Kim, Y. Seo, S.Y. Kim, H. Lee, Combined hybrid structure of siRNA tailed IVT mRNA (ChriST mRNA) for enhancing DC maturation and subsequent anticancer T cell immunity, J. Controlled Release 327 (2020) 225–234, https://doi.org/10.1016/j.jconrel.2020.08.009.

[48] B. Jang, B. Kim, H. Kim, H. Kwon, M. Kim, Y. Seo, M. Colas, H. Jeong, E.H. Jeong, K. Lee, H. Lee, Enzymatic synthesis of self-assembled Dicer substrate RNA nanostructures for programmable gene silencing, Nano Lett. 18 (2018) 4279–4284, https://doi.org/10.1021/acs.nanolett.8b01267.

[49] K.-H. Lee, S.-E. Min, H. Kim, S.-G. Lee, D.-M. Kim, A molecular nanodevice for targeted degradation of mRNA during protein synthesis, Sci. Rep. 6 (2016) 20733, https://doi.org/10.1038/srep20733.

[50] K. Yehl, A. Mugler, S. Vivek, Y. Liu, Y. Zhang, M. Fan, E.R. Weeks, K. Salaita, High-speed DNA-based rolling motors powered by RNase H, Nat. Nanotechnol. 11 (2016) 184–190, https://doi.org/10.1038/nnano.2015.259.

[51] W. Wang, M. Shu, A. Nie, H. Han, Ultrasensitive evaluation of Ribonuclease H activity using a DNAzyme-powered on-particle DNA walker, Sens. Actuators B Chem. 304 (2020) 127380, https://doi.org/10.1016/j.snb.2019.127380.

[52] T.A. Steitz, J.A. Steitz, A general two-metal-ion mechanism for catalytic RNA, Proc. Natl. Acad. Sci. USA 90 (1993) 6498–6502, https://doi.org/10.1073/pnas.90.14.6498.

[53] J.L. Keck, E.R. Goedken, S. Marqusee, Activation/attenuation model for RNase H: a one-metal mechanism with second-metal inhibition, J. Biol. Chem. 273 (1998) 34128–34133, https://doi.org/10.1074/jbc.273.51.34128.

[54] H.H. Hogrefe, R.I. Hogrefe, R.Y. Walder, J.A. Walder, Kinetic analysis of Escherichia coli RNase H using DNA-RNA-DNA/DNA substrates, J. Biol. Chem. 265 (1990) 5561–5566, https://doi.org/10.1016/S0021-9258(19)39397-4.

[55] H. Inoue, Y. Hayase, S. Iwai, E. Ohtsuka, Sequence-dependent hydrolysis of RNA using modified oligonucleotide splints and RNase H, FEBS Lett. 215 (1987) 327–330, https://doi.org/10.1016/0014-5793(87)80171-0.

[56] W.F. Lima, J.B. Rose, J.G. Nichols, H. Wu, M.T. Migawa, T.K. Wyrzykiewicz, A. M. Siwkowski, S.T. Crooke, Human RNase H1 discriminates between subtle variations in the structure of the heteroduplex substrate, Mol. Pharmacol. 71 (2007) 83–91, https://doi.org/10.1124/mol.106.025015.

[57] H. Lee, H. Cho, J. Kim, S. Lee, J. Yoo, D. Park, G. Lee, RNase H is an exo- and endoribonuclease with asymmetric directionality, depending on the binding mode to the structural variants of RNA:DNA hybrids, Nucleic Acids Res. 50 (2022) 1801–1814, https://doi.org/10.1093/nar/gkab1064.

[58] Z. Cui, J.A. Theruvathu, A. Farrel, A. Burdzy, L.C. Sowers, Characterization of synthetic oligonucleotides containing biologically important modified bases by matrix-assisted laser desorption/ionization time-of-flight mass spectrometry, Anal. Biochem. 379 (2008) 196–207, https://doi.org/10.1016/j.ab.2008.04.031.

[59] I.G. Gut, Depurination of DNA and matrix-assisted laser desorption/ionization mass spectrometry, Int. J. Mass Spectrom. Ion Proc. 169 (1997) 313–322, https://doi.org/10.1016/S0168-1176(97)00208-5.

[60] E. Nordhoff, R. Cramer, M. Karas, F. Hillenkamp, F. Kirpekar, K. Kristiansen, P. Roepstorff, Ion stability of nucleic acids in infrared matrix-assisted laser desorption/ionization mass spectrometry, Nucleic Acids Res. 21 (1993) 3347–3357, https://doi.org/10.1093/nar/21.15.3347.

[61] E. Nordhoff, F. Kirpekar, P. Roepstorff, Mass spectrometry of nucleic acids, Mass Spectrom. Rev. 15 (1996) 67–138, 10.1002/(SICI)1098-2787(1996)15:2<67::AID-MAS1>3.0.CO;2-8.

[62] A. Vidyasagar, N.A. Wilson, A. Djamali, Heat shock protein 27 (HSP27): biomarker of disease and therapeutic target, Fibrogenesis Tissue Repair 5 (2012) 1–7, https://doi.org/10.1186/1755-1536-5-7.

[63] J. Kao, J.R. Pollack, RNA interference-based functional dissection of the 17q12 amplicon in breast cancer reveals contribution of coamplified genes, Genes. Chromosomes, Cancer 45 (2006) 761–769, https://doi.org/10.1002/gcc.20339.

[64] F. Martorana, G. Motta, G. Pavone, L. Motta, S. Stella, S.R. Vitale, L. Manzella, P. Vigneri, AKT inhibitors: new weapons in the fight against breast cancer? Front. Pharmacol. 12 (2021) 662232 https://doi.org/10.3389/fphar.2021.662232.

[65] Y. Kim, M. Jo, J. Schmidt, X. Luo, T.P. Prakash, T. Zhou, S. Klein, X. Xiao, N. Post, Z. Yin, A.R. MacLeod, Enhanced potency of GalNAc-conjugated antisense oligonucleotides in hepatocellular cancer models, Mol. Ther. 27 (2019) 1547–1557, https://doi.org/10.1016/j.ymthe.2019.06.009.

[66] S.L. Beaucage, M.H. Caruthers, Deoxynucleoside phosphoramidites—A new class of key intermediates for deoxypolynucleotide synthesis, Tetrahedron Lett. 22 (1981) 1859–1862, https://doi.org/10.1016/S0040-4039(01)90461-7.